Asian Journal of Chemistry; Vol. 38, No. 11 (2026), 2938-2946
ASIAN JOURNAL OF CHEMISTRY
https://doi.org/10.14233/ajchem.2026.36778

# Design, Synthesis, Biological Evaluation, Molecular Docking, Pharmacophore Modelling and 3D-QSAR Analysis of Novel Substituted Imidazolidine Derivatives as Potential Antimicrobial Agents

PRIYANKA YADAV*, and NEERAJ UPMANYU

Department of Pharmaceutical Sciences, Sanjeev Agrawal Global Educational University, Katara Hill Extension, Bhopal-462023, India

*Corresponding author: E-mail: priyankaya.9889@gmail.com

*Received*: 5 July 2026 *Accepted*: 5 October 2026 *Published online*: 13 November 2026 AJC-22525

The present study reports the combined experimental and computational approaches to investigate the antimicrobial potential of 104 structurally diverse substituted imidazolidine derivatives. Selected compounds were synthesized based on their docking results and characterized by IR, $^{1}$H NMR and $^{13}$C NMR spectroscopy and mass spectrometry. Their antimicrobial activity was assessed *in vitro* against selected bacterial and fungal strains. Among the tested compounds, derivatives **47** and **52** exhibited the strongest activity, with compound **47** showing antibacterial activity comparable to that of amoxicillin. Molecular docking studies against lanosterol 14α-demethylase (CYP51; PDB ID: 1E9X) were performed to explore the possible interactions of the compounds within the enzyme-binding pocket. Compounds **47** and **52** achieved docking scores of -10.4 and -10.3 kcal/mol, respectively, while compounds **15**, **18** and **21** each recorded a score of -10.2 kcal/mol. The docked complexes exhibited hydrogen bonding, π-π stacking, π-cation, π-alkyl and hydrophobic interactions. Pharmacophore modelling identified one hydrogen-bond acceptor feature, one hydrophobic feature and three aromatic-ring features associated with the activity profile. The optimized three-dimensional quantitative structure–activity relationship (3D-QSAR) model yielded an ($R^2$) value of 0.6682, a ($Q^2$) value of 0.3463, a Pearson correlation coefficient of 0.7497 and a stability value of 0.847. Analysis of the steric, electrostatic and hydrophobic contour maps provided further insight into the influence of substituent identity and spatial arrangement on antimicrobial activity. The experimental findings identify compounds **47** and **52** as promising candidates for further optimization of imidazolidine-based antimicrobial agents.

**Keywords: Imidazolidine, 3D-QSAR, Antimicrobial activity, Molecular docking, CYP51.**

## INTRODUCTION

Heterocyclic compounds represent an important class of biologically active molecules and form the structural basis of many therapeutic agents [1]. Among them, imidazolidine derivatives have attracted interest in medicinal chemistry due to their structural diversity and potential pharmacological applications. Imidazolidine is a five-membered saturated heterocyclic ring containing two nitrogen atoms. The nature and position of its substituents can influence molecular polarity, hydrogen-bonding capacity and interactions with biological targets [2,3]. Modifications to this ring system offer opportunities to investigate structure-activity relationships (SAR) and identify compounds with improved biological properties. Imidazolidine derivatives and related compounds have been investigated for antimicrobial, antifungal, anticonvulsant, anticancer, antiparasitic, analgesic, antitubercular and antiviral activities [4]. The broader medicinal importance of nitrogen-containing heterocycles is evident in biologically important molecules such as vitamin $B_{12}$, vitamin $B_6$, biotin and histamine, although these compounds possess distinct heterocyclic frameworks [5]. Several established antifungal agents, such as ketoconazole, miconazole, clotrimazole, econazole and tioconazole, contain imidazole or related azole groups.

Fungal infections caused by *Candida*, *Aspergillus* and *Cryptococcus* species pose a significant clinical challenge, particularly in immunocompromised patients [6]. The emergence of antifungal resistance has increased the need for compounds with improved potency and activity against resistant fungal strains. Lanosterol 14α-demethylase (CYP51), a cytochrome P450 enzyme involved in ergosterol biosynthesis, is an established target of several azole antifungal agents [7,8]. CYP51 catalyses the removal of the 14 α-methyl group from sterol precursors during ergosterol biosynthesis. The

This is an open access journal, and articles are distributed under the terms of the Attribution 4.0 International (CC BY 4.0) License. This license lets others distribute, remix, tweak, and build upon your work, even commercially, as long as they credit the author for the original creation. You must give appropriate credit, provide a link to the license, and indicate if changes were made.

inhibition of this enzyme disrupts sterol production and alters fungal membrane composition and function, which can impair cellular growth. The changes in sterol metabolism are central to the antifungal action of established CYP51 inhibitors. Investigating the interactions of new chemical entities with this enzyme may help identify potential antifungal candidates [9].

Antimicrobial resistance (AMR) poses a major public health challenge by reducing the effectiveness of existing treatments [10]. The development of new antimicrobial agents and the identification of structural features associated with their activity remain important goals in medicinal chemistry. Substituted nitrogen-containing heterocycles offer a promising framework for exploring new antimicrobial candidates. Previous investigations have explored substituted imidazolidines, imidazole-containing molecular hybrids and related azole derivatives for their biological activities [3,7,11]. The computational methods such as molecular docking, pharmacophore modelling and three-dimensional quantitative structure activity relationship (3D-QSAR) analysis can complement experimental testing by examining potential target interactions and identifying molecular features associated with activity. Their combined application may help clarify the influence of substituent identity, electronic characteristics and spatial arrangement on biological performance.

In the present study, 104 structurally diverse substituted imidazolidine derivatives were evaluated computationally for their potential antimicrobial activity and selected compounds were synthesized and tested *in vitro* against selected bacterial and fungal strains. The molecular docking was performed against lanosterol 14α-demethylase (CYP51; PDB ID: 1E9X) to examine potential binding orientations and interactions within the enzyme binding pocket [12]. Pharmacophore modelling and 3D-QSAR analysis were performed to identify the key structural and physico-chemical features influencing antimicrobial activity. Steric, electrostatic and hydrophobic effects were assessed to establish preliminary structure-activity relationships (SARs) and prioritize promising derivatives for further optimization.

## EXPERIMENTAL

All chemicals and reagents used in the synthesis of imidazolidine derivatives were of analytical grade and procured from Sigma-Aldrich and Fisher Scientific. Benzil, substituted aldehydes, substituted anilines and ammonium acetate were used as received in the one-pot three-component condensation reaction, with absolute ethanol as the solvent. The synthesized compounds were purified by column chromatography using silica gel (0.063-0.2 mm). Their purity was assessed by thin-layer chromatography (TLC) on aluminium-backed silica gel $F_{254}$ plates, with spots visualized under iodine vapour. Ketoconazole (standard antifungal drug) and dimethyl sulfoxide (DMSO) (negative control drug) were purchased from Sigma-Aldrich. The fungal strains *Candida albicans*, *Aspergillus niger* and *Cryptococcus neoformans* were procured from the American Type Culture Collection (ATCC, Manassas, USA). Sabouraud dextrose agar (SDA) and Sabouraud dextrose broth (SDB) were provided by Sigma-Aldrich. Culture media, glassware and reagents were all sterilized before use and the antifungal testing was carried out under sterile conditions.

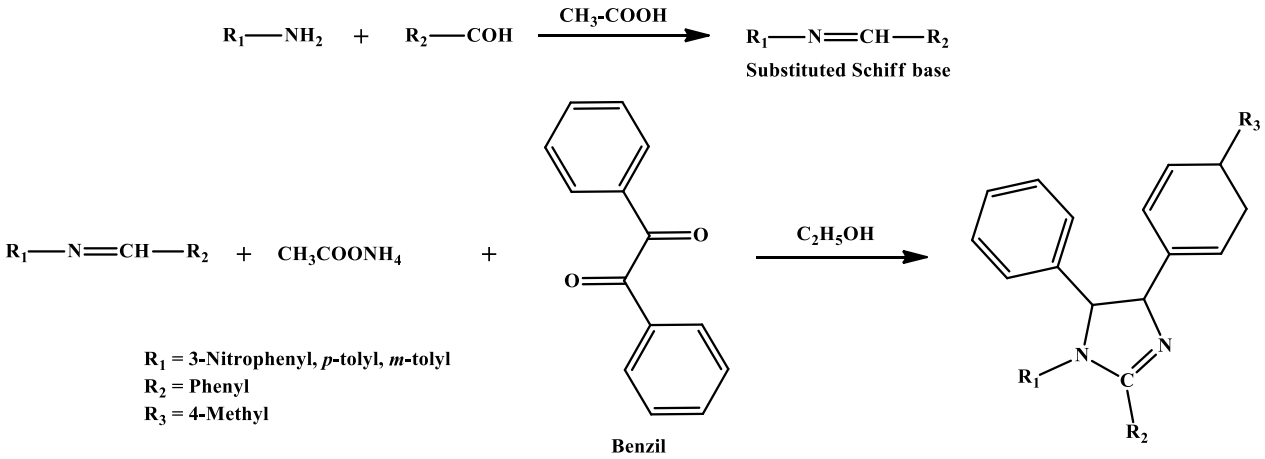
The synthesized imidazolidine derivatives were characterized using physico-chemical and spectroscopic methods. The reaction progress and product purity were monitored by thin-layer chromatography (TLC) on silica gel G plates using toluene-ethyl acetate-formic acid (5:4:1, v/v/v) or benzene-acetone (9:1, v/v) as the mobile phase. Spots were visualized under UV light at 254 and 365 nm or by exposure to iodine vapour and the corresponding $R_f$ values were recorded. Melting points were determined by the open-capillary method using a digital melting-point apparatus and are reported as uncorrected values. IR spectra were recorded using KBr pellets and $^1$H NMR spectra were obtained on a Bruker 400 MHz spectrometer using DMSO-$d_6$ as the solvent and TMS as the internal standard. Electrospray ionization mass spectrometry (ESI-MS) was used to confirm molecular masses.

**General procedure for the synthesis of substituted imidazolidine derivatives:** Substituted imidazolidine derivatives were synthesized by a one-pot multicomponent condensation reaction. Benzil (1 mmol) and the appropriate substituted aromatic aldehyde (1 mmol) were dissolved in absolute ethanol followed by the addition of ammonium acetate (5 mmol) and substituted aniline (1 mmol), where applicable. The reaction mixture was refluxed at 80-90 ºC for 4-6 h and monitored by TLC using hexane-ethyl acetate (7:3) as the mobile phase (**Scheme-I**). After completion, the mixture was cooled to room temperature and cold distilled water was added to precipitate the product [13]. The solid was further cooled in an ice bath, collected by vacuum filtration, washed with cold ethanol, dried and finally recrystallized.

**2,4,5-Triphenyl-1-(*m*-tolyl)imidazolidine (47):** White crystalline, yield: 72%, m.p.: 188-190 ºC, $R_f$: 0.62 (ethyl acetate: hexane 7:3); m.f.: $C_{28}H_{26}N$ (*m.w.*: 390.21); IR (KBr, $\nu_{max}$, $cm^{-1}$): 3303 (N–H), 2993 (C–H), 1600 (arom. skeletal vibration), 1438 (C–H *bend*.), 1328 and 1088 (C–N/ring *vibr*.), 879 (*arom*. C–H out-of-plane bending), 540, 520, 508, 498, 458, 440, 419; $^1$H NMR (400 MHz, DMSO-$d_6$, δ ppm): 2.25 (s, 3H, Ar–$CH_3$), 6.90-7.65 (m, 19H, Ar–H), 8.12 (br s, 1H, NH). ESI-MS (*m/z*): 391 $[M]^+$, 190, 149, 134, 119, 105, 91 (base peak), 77.

**1-(3-Nitrophenyl)-4,5-diphenyl-2-(*p*-tolyl)imidazolidine (52):** Off white crystalline, yield: 68%, m.p.: 202-205 ºC, $R_f$: 0.58 (chloroform:methanol 8:2); m.f.: $C_{28}H_{25}N_3O_2$ (*m.w.*: 435.19); IR (KBr, $\nu_{max}$, $cm^{-1}$): 3087, 2978, 2947, 2880 (C–H), 1615 and 1584 (arom. skeletal vibrations), 1532 ($NO_2$ asym. *str*.), 1445, 1394, 1315, 1273 ($NO_2$/C–N *vibr*.), 1200, 1158, 1085, 1035, 933, 813, 721, 666, 591, 559, 532, 508; $^1$H NMR (400 MHz, DMSO-$d_6$, δ ppm): 2.28 (s, 3H, Ar–$CH_3$), 3.50 (br s, 1H, NH), 3.95 and 4.42 (2H, imidazolidine CH), 6.80-8.20 (m, Ar–H); ESI-MS (*m/z*): 450 $[M]^+$, 190, 149, 134, 119, 105, 91 (base peak), 77.

**4,5-Diphenyl-1,2-di-(*p*-tolyl)imidazolidine (15):** Yellow crystalline, yield: 75%, m.p.: 176-178 ºC, $R_f$: 0.65 (ethyl acetate: hexane 6:4); m.f.: $C_{29}H_{28}N_2$ (*m.w.*: 404.23); IR (KBr, $\nu_{max}$, $cm^{-1}$): 3304, 3243 (N–H), 2973, 2721 (C–H), 1600, 1500, 1438 (Ar C=C), 1351, 1308, 1200 (C–N), 1088, 1030 (Ar C–H in-plane *bend*.), 921, 905, 879, 813, 732 (Ar C–H out-of-plane *bend*.),




**Scheme-I:** Proposed synthetic pathway for the synthesis of substituted imidazole derivatives

535 (arom. skeletal vibration); $^1$H NMR (400 MHz, DMSO-$d_6$, δ ppm): 2.28 (s, 6H, 2 × Ar–$CH_3$), 3.92 (d, 1H, CH-imidazolidine), 4.45 (d, 1H, CH-imidazolidine), 5.10 (br s, 1H, NH), 6.80-7.60 (m, 18H, Ar–H); ESI-MS (*m/z*): 419 $[M]^+$, 190, 149, 134, 119, 105, 91 (base peak), 77.

**4,5-Diphenyl-1-(*m*-tolyl)-2-(*p*-tolyl)imidazolidine (21):** White amorphous, yield: 70%, m.p.: 210-212 ºC, $R_f$: 0.55 (Toluene:ethyl acetate 7:3); m.f.: $C_{29}H_{28}N_2$ (*m.w.*: 404.23); IR (KBr, $\nu_{max}$, $cm^{-1}$): 3322 (N–H), 2944, 2832 (C–H), 1660, 1448, 1415 (Ar C=C), 1113 (C–N), 1020 (Ar C–H in-plane bending), 614, 445, 423, 407 (arom. skeletal vibrations); $^1$H NMR (400 MHz, DMSO-$d_6$, δ ppm): 2.30 (s, 6H, 2 × Ar–$CH_3$), 3.92 (d, 1H, CH-imidazolidine), 4.48 (d, 1H, CH-imidazolidine), 5.25 (br s, 1H, NH), 6.50-7.60 (m, 18H, Ar–H); ESI-MS (*m/z*): 391 $[M]^+$, 190, 149, 134, 119, 105, 91 (base peak), 77.

**Antimicrobial activity:** The antimicrobial activity of the synthesized imidazolidine derivatives was evaluated against selected bacterial and fungal strains using the agar well diffusion and broth microdilution methods [14]. The bacterial strains *viz*. *Staphylococcus aureus* ATCC 25923, *Escherichia coli* ATCC 25922 and *Pseudomonas aeruginosa* ATCC 27853. Antifungal activity was tested against *Candida albicans* MTCC 227, *Aspergillus niger* MTCC 282 and *Cryptococcus neoformans* MTCC 7688. Stock solutions of the compounds were prepared in DMSO at 10 mg/mL and diluted to the required concentrations [15]. Fresh microbial cultures were used to prepare inocula adjusted to the 0.5 McFarland turbidity standard. Mueller-Hinton agar was used for bacterial testing, while Sabouraud dextrose agar or potato dextrose agar was used for fungal testing [16].

For the agar well diffusion assay, sterile agar plates were inoculated with standardized microbial suspensions and 6 mm wells were prepared aseptically. Each well received 50 µL of the test solution [17]. Fluconazole was used as the antifungal positive control, and appropriate standard antibacterial agents were used as positive controls. DMSO served as the negative control. Bacterial plates were incubated for 18-24 h at 35 ± 2 ºC, while fungal plates were incubated for 48-72 h at 28 ± 2 ºC. Antimicrobial activity was assessed by measuring the inhibition zones in millimetres [18].

Minimum inhibitory concentrations (MICs) were determined by broth microdilution following the stated CLSI guidelines. Two-fold serial dilutions of the compounds ranging from 3.125 to 200 µg/mL were prepared in sterile broth and inoculated with standardized microbial suspensions [19]. After incubation, the MIC was recorded as the lowest concentration that completely inhibited visible microbial growth. Each experiment was performed in triplicate and results were expressed as mean ± standard deviation (SD). Statistical significance was assessed by one-way analysis of variance (ANOVA) with $p < 0.05$ considered statistically significant [20].

**Molecular docking studies:** Molecular docking studies were carried out to investigate the binding interactions of the synthesized imidazolidine derivatives with lanosterol 14α-demethylase (CYP51), a key enzyme involved in fungal ergosterol biosynthesis [21]. The crystal structure of cytochrome P450 14α-sterol demethylase complexed with 4-phenylimidazolidine (PDB ID: 1E9X) was retrieved from the Protein Data Bank (PDB) [22].

**Ligand preparation:** The chemical structures of the synthesized imidazolidine derivatives were constructed using Avogadro molecular modeling software [23]. All structures were subjected to geometry optimization using the universal force field (UFF) through the auto optimization module until the minimum energy conformation was achieved. The optimized structures were subsequently saved in suitable formats for docking analysis [24].

**Protein preparation:** Protein preparation was performed using BIOVIA Discovery Studio Visualizer 2020. The downloaded protein structure was processed by removing crystallographic water molecules and co-crystallized ligands [25]. Polar hydrogen atoms were added and the active binding site was identified based on the coordinates of the native ligand. The receptor structure was subsequently prepared for docking calculations and saved in the appropriate format [26].

**Docking protocol:** The docking of the molecule to the enzyme was done through AutoDock Vina as part of MGL Tools package. Before docking [27], both receptor and ligand structures were converted into PDBQT format. During protein preparation, coordinates were given and a grid box that includes the active site residues was created. Molecular docking simu-

lations were performed using the default parameters and the binding affinities were expressed in kcal/mol [28]. The docked poses were ranked according to their binding energies, with the conformation exhibiting the lowest binding energy selected as the most favourable pose. The interactions between the protein and ligand, including hydrogen bonding, hydrophobic interactions, π-π stacking, π-cation, π-alkyl and van der Waals interactions, were analyzed using Discovery Studio Visualizer [28,29].

**Pharmacophore modelling:** To understand the key structural features that impart the antimicrobial activity to the synthesized imidazolidine derivatives [30], Pharmacophore modelling was carried out. Discovery Studio software was used to generate common pharmacophore hypotheses for set of biologically active compounds using HypoGen algorithm. A hydrogen bond acceptors (A), hydrogen bond donors (D) and hydrophobic regions (H), aromatic ring features (R) and positive ionizable centers (P) were examined when generating models. Several hypotheses were developed and tested using survival score, vector score, volume score and alignment quality. The successful pharmacophore model was chosen on the basis of maximum mapping of the most active compounds and explanation of the activity [31].

**3D-QSAR analysis:** analysis was performed using PHASE in the Schrödinger molecular modelling suite to investigate the relationship between the structural features of the synthesized imidazolidine derivatives and their antimicrobial activity [32]. The activity values were log-transformed and the compounds were divided into training and test sets using a rational randomization approach. The training set was used to develop the QSAR model, while the test set was reserved for external validation [33]. Partial least squares (PLS) regression was employed to construct the model and its performance was evaluated using $R^2$, $Q^2$, root mean square error (RMSE), Pearson correlation coefficient (r), stability index (SI) and F-statistic. The model incorporated five pharmacophoric features, *viz*. hydrogen-bond acceptor (A), hydrogen-bond donor (D), hydrophobic region (H), positively ionizable feature (P) and aromatic ring (R). Steric, electrostatic and hydrophobic contour maps were generated to visualize the structural regions associated with changes in activity and to interpret the structure activity relationships of the synthesized compounds [34,35]. These analyses were used to identify key molecular features that may influence inhibitory activity against lanosterol 14α-demethylase (CYP51) and to suggest potential structural modifications for designing analogues with improved predicted activity.

## RESULTS AND DISCUSSION

The optimized reaction conditions were applied to the synthesis of the substituted imidazolidine derivatives using a one-pot multicomponent condensation of benzil, substituted aromatic aldehydes, primary amines and ammonium acetate in refluxing ethanol (**Scheme-I**). A possible reaction pathway involves the initial formation of a Schiff-base intermediate from the substituted aldehyde and primary amine followed by further condensation and cyclization involving benzil and ammonium acetate. The products were isolated as white to pale-yellow crystalline solids. The compounds showed good solubility in ethanol and DMSO but limited solubility in water. These differences may be associated with variations in molecular structure and the nature of the substituents on the aromatic rings.

***In vitro* antibacterial activity:** The antibacterial activity of the synthesized imidazolidine derivatives was evaluated against five Gram-positive bacterial strains (*S. aureus*, *B. subtilis*, *E. faecalis*, *S. pyogenes* and *L. monocytogenes*) and five Gram-negative strains (*E. coli*, *P. aeruginosa*, *S. typhi*, *K. pneumoniae* and *S. dysenteriae*) using the agar well diffusion method. Ampicillin and ciprofloxacin served as reference drugs for Gram-positive and Gram-negative bacteria, respectively, while DMSO was used as the negative control. The results (Table-1) indicate a concentration-dependent response, with larger inhibition zones generally observed at higher concentrations (25-100 μg/mL). Among the tested derivatives compound **47** and **52** exhibited the strongest antibacterial activity. Compound **47** produced inhibition zones of 21-23 mm against Gram-positive bacteria and 17-19 mm against Gram-negative bacteria, with reported MIC values of 12.5

TABLE-1
*In vitro* ANTIBACTERIAL ACTIVITY DATA OF SYNTHESIZED IMIDAZOLIDINE DERIVATIVES AT DIFFERENT CONCENTRATIONS (ZONE OF INHIBITION IN mm)

| Compound | Conc. (μg/mL) | *S. aureus* | *B. subtilis* | *E. faecalis* | *S. pyogenes* | *L. monocytogenes* | *E. coli* | *P. aeruginosa* | *K. pneumoniae* | *S. typhi* | *S. dysenteriae* |
|---|---|---|---|---|---|---|---|---|---|---|---|
| **47** | 25 | 14 | 13 | 12 | 13 | 12 | 12 | 10 | 11 | 12 | 11 |
| | 50 | 19 | 18 | 17 | 18 | 17 | 16 | 14 | 15 | 16 | 15 |
| | 100 | 23 | 22 | 21 | 22 | 21 | 19 | 17 | 18 | 18 | 17 |
| **52** | 25 | 13 | 12 | 12 | 12 | 11 | 11 | 10 | 10 | 11 | 10 |
| | 50 | 18 | 17 | 17 | 17 | 16 | 15 | 13 | 14 | 15 | 14 |
| | 100 | 22 | 21 | 20 | 21 | 20 | 18 | 16 | 17 | 17 | 16 |
| **15** | 25 | 11 | 10 | 10 | 10 | 9 | 9 | 8 | 8 | 9 | 8 |
| | 50 | 16 | 15 | 15 | 15 | 14 | 13 | 11 | 12 | 13 | 12 |
| | 100 | 20 | 19 | 19 | 19 | 18 | 16 | 14 | 15 | 16 | 14 |
| **21** | 25 | 9 | 9 | 8 | 9 | 8 | 8 | 7 | 7 | 8 | 7 |
| | 50 | 14 | 13 | 13 | 13 | 12 | 11 | 10 | 11 | 12 | 10 |
| | 100 | 18 | 17 | 17 | 17 | 16 | 14 | 12 | 13 | 14 | 12 |
| Ampicillin (Std.) | 25-100 | 18-28 | 18-28 | 18-28 | 18-28 | 18-28 | – | – | – | – | – |

and 25 μg/mL, respectively. Compound **52** showed comparable activity and similar MIC values. Compound **15** displayed moderate activity, with inhibition zones of 15-20 mm against Gram-positive strains and 12-17 mm against Gram-negative strains at the highest tested concentration. Its MIC values ranged from 25 to 50 μg/mL against both groups. Compound **21** was less active, producing inhibition zones of 14-19 mm and 11-16 mm against Gram-positive and Gram-negative bacteria, respectively, with an MIC value of 50 μg/mL. The remaining derivatives showed weaker effects, generally exhibiting inhibition zones of 12 mm or less and MIC values above 100 μg/mL.

The synthesized compounds were generally more active against Gram-positive than Gram-negative bacteria, possibly due to differences in cell-envelope permeability and efflux mechanisms. Among the Gram-negative strains *E. coli* and *S. typhi* were more susceptible than *P. aeruginosa* and *K. pneumoniae*. Compounds **47** and **52** showed the strongest antibacterial activity, although the reference drugs were more potent, with ampicillin and ciprofloxacin exhibiting inhibition zones of 25-28 mm and 22-25 mm, respectively and MIC values of 6.25 μg/mL.

***In vitro* antifungal activity:** The antifungal activity of the synthesized imidazolidine derivatives was evaluated against *C. albicans*, *A. niger* and *C. neoformans* using the agar well diffusion method at concentrations of 25, 50 and 100 μg/mL. Ketoconazole served as the reference drug and DMSO as the negative control. The compounds exhibited concentration-dependent inhibition, with **47** and **52** showing the strongest activity. At 100 μg/mL compound **47** produced inhibition zones of 22, 21 and 20 mm against the three fungal strains, respectively, while compound **52** produced zones of 21, 20 and 18 mm (Table-2). Compound **15** showed moderate activity with inhibition zones of 20, 19 and 18 mm and a reported MIC of 25 μg/mL. Compound **21** was less active, with inhibition zones of 15-19 mm and an MIC of 50 μg/mL. The remaining derivatives showed weaker activity with inhibition zones below 15 mm and MIC values above 50 μg/mL. *C. albicans* was the most susceptible strain followed by *A. niger* and *C. neoformans*. Ketoconazole remained more potent, exhibiting inhibition zones of 25, 23 and 22 mm, respectively, with an MIC of 6.25 μg/mL.

TABLE-2
*In vitro* ANTIFUNGAL ACTIVITY DATA OF SYNTHESIZED IMIDAZOLIDINE DERIVATIVES AT DIFFERENT CONCENTRATIONS (ZONE OF INHIBITION IN mm)

| Compound | Conc. (μg/mL) | *C. albicans* | *A. niger* | *C. neoformans* |
|---|---|---|---|---|
| **47** | 25 | 12 | 11 | 10 |
| | 50 | 17 | 16 | 15 |
| | 100 | 22 | 21 | 20 |
| **52** | 25 | 11 | 10 | 9 |
| | 50 | 16 | 15 | 14 |
| | 100 | 21 | 20 | 18 |
| **15** | 25 | 10 | 9 | 8 |
| | 50 | 15 | 14 | 13 |
| | 100 | 20 | 19 | 18 |
| **21** | 25 | 8 | 7 | 7 |
| | 50 | 13 | 12 | 11 |
| | 100 | 18 | 16 | 15 |
| Ketoconazole (Std.) | 25 | 15 | 14 | 14 |
| | 50 | 20 | 19 | 18 |
| | 100 | 25 | 23 | 22 |

**Molecular docking studies:** Molecular docking studies were performed against fungal lanosterol 14α-demethylase (CYP51; PDB ID: 1E9X), an enzyme involved in ergosterol biosynthesis, to assess the predicted binding affinity of the synthesized imidazolidine derivatives. The docking scores ranged from -7.1 to -10.4 kcal/mol, with compounds **47**, **52**, **15** and **21** exhibiting the most favourable scores (Table-3 and Fig. 1). Compound **47** showed the lowest docking score (-10.4 kcal/mol), followed by compound **52** (-10.3 kcal/mol) and compounds **15** and **21** (-10.2 kcal/mol each). Protein–ligand interaction analysis identified several non-covalent interactions within the predicted CYP51 binding pocket, which include the conventional and carbon–hydrogen bonding, van der Waals forces, π-cation, π-sigma, π-alkyl, π-π stacking, π-π T-shaped and carbon–alkyl interactions. These interactions may contribute to the predicted stability of the docked complexes. Substituent effects were observed across the series, with some chlorine- and nitro-containing derivatives showing more favourable docking scores than their unsubstituted analogues. These substituents may influence ligand binding through changes in hydrophobic and other non-covalent interactions. The favourable docking scores of compounds **47** and **52** were consistent with their comparatively strong antifungal activity in the experimental screening. This agreement provides a basis for further investigation of their possible interaction with CYP51.

TABLE-3
MOLECULAR DOCKING SCORES OF SELECTED IMIDAZOLIDINE DERIVATIVES WITH CYTOCHROME P450 14α-STEROL DEMETHYLASE PROTEIN (PDB: 1E9X)

| Compound | Docking score | Compound | Docking score |
|---|---|---|---|
| **47** | -10.4 | **56** | -9.9 |
| **52** | -10.3 | **101** | -9.9 |
| **15** | -10.2 | **8** | -9.8 |
| **21** | -10.2 | **10** | -9.8 |
| **18** | -10.2 | **73** | -9.8 |
| **58** | -10.1 | **75** | -9.8 |
| **23** | -10.1 | **95** | -9.8 |
| **41** | -10.1 | **20** | -9.7 |
| **85** | -10.1 | **22** | -9.7 |
| **53** | -9.9 | **59** | -9.7 |

**Pharmacophore hypotheses:** Twenty pharmacophore hypotheses were generated to identify the key structural features associated with the biological activity of the synthesized compounds. The hypotheses incorporated five pharmacophoric features: hydrogen-bond acceptor (A), hydrogen-bond donor (D), hydrophobic region (H), positively ionizable feature (P) and aromatic ring (R). Based on the ranking and ligand alignment, the five highest-ranked hypotheses were AHRRR_2, HPRRR_3, HPRR_2, HHRRR_1 and PRRR_2. Among these, AHRRR_2 comprised one hydrogen-bond acceptor, one hydrophobic region and three aromatic ring features, as shown in Fig. 2a-c. This hypothesis represents the spatial arrangement

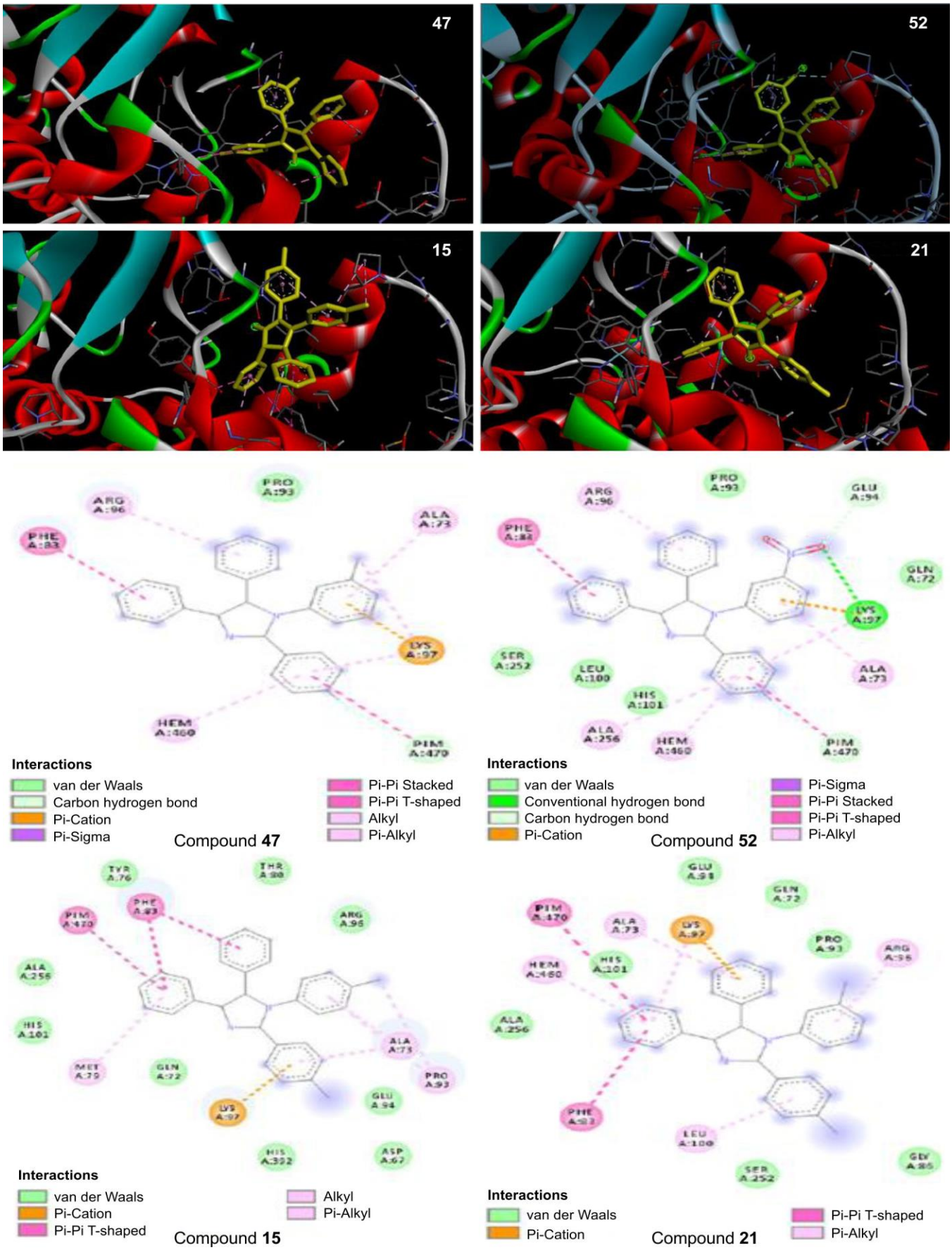



Fig. 1. 2D & 3D Docking interaction poses of selected compounds with protein 1E9X

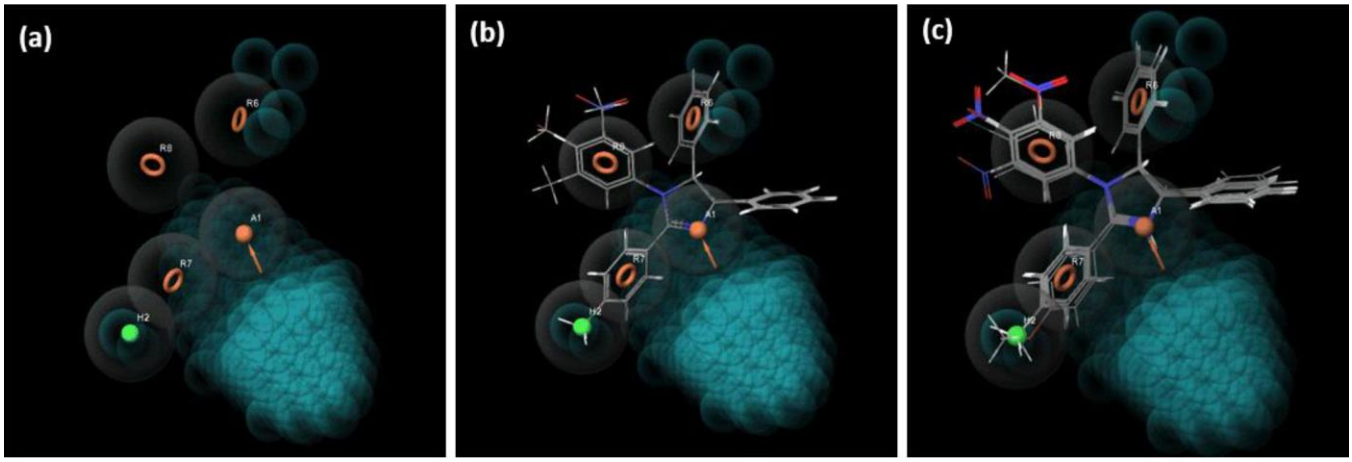



Fig. 2. Best pharmacophore hypothesis: (a) AHRRR_2; (b) AHRRR_2 mapped with active ligands; and (c) AHRRR_2 mapped with inactive ligands

of pharmacophoric features that may contribute to ligand activity and provide a basis for further structure–activity relationship analysis.

**3D QSAR analysis:** The PLS 7 model was selected for 3D-QSAR analysis based on its statistical parameters for example, SD (0.4753), $R^2$ (0.6682), $R^2$CV (0.5359), $R^2$ scramble (0.3827), stability (0.847), F value (4), P value (0.112), RMSE (0.58), $Q^2$ (0.3463) and Pearson correlation coefficient (0.7497) (Table-4). Models with increasing numbers of PLS components were evaluated to identify a suitable model while limiting the risk of overfitting. The selected model was developed using a randomly selected training set comprising 85% of the data. Compound **23**, with an experimental activity of 6.31 and a predicted activity of 6.3639 (Table-5), was used as the reference molecule for visualizing and interpreting the steric, electrostatic and hydrophobic contour maps generated by the model. The close agreement between its experimental and predicted activity provides an illustrative example of the model's prediction for this compound.

**Steric contour map:** Fig. 3 shows the steric contour map generated using ligand **23** as the reference structure. The green contours near the *meta*-fluoro substituent of the N1-linked phenyl ring and the *p*-tolyl group attached at C2 indicate regions where steric bulk may favour antifungal activity. The yellow regions mark positions where additional bulk may be less favourable. These findings suggest that substituent size and spatial arrangement may influence the activity of the imidazolidine derivatives.

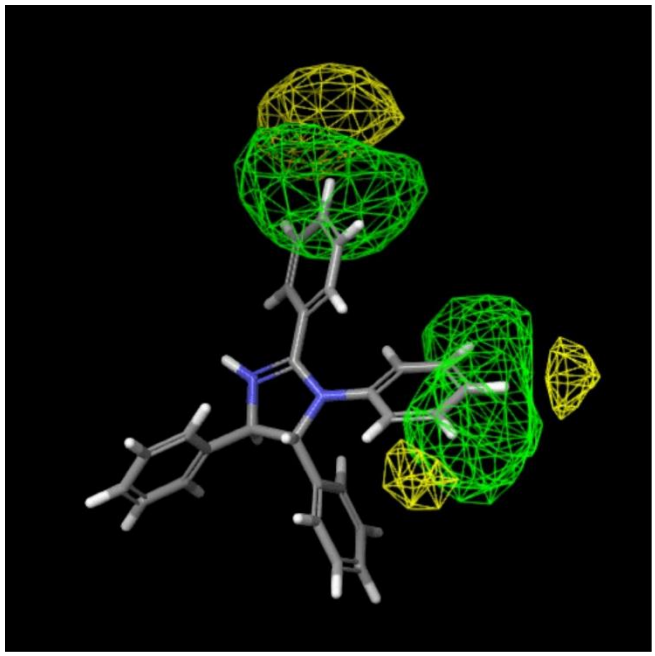


Fig. 3. 3D Gaussian steric map showing the spatial distribution of steric features around ligand 23

**Electrostatic contour map:** Fig. 4 shows the electrostatic contour map for ligand **23**. The blue contours near N3, the phenyl group attached at C2 and the phenyl ring linked to N1 indicate regions where electrostatic properties may favour

TABLE-4
VALIDATION STATISTICS AND PREDICTIVE PERFORMANCE PARAMETERS OF PLS BASED QSAR-MODELS FROM VARYING NUMBER OF LATENT FACTORS

| PLS factor | SD | $R^2$ | $R^2$ CV | $R^2$ scramble | Stability | F | P | RMSE | $Q^2$ | Pearson-r |
|---|---|---|---|---|---|---|---|---|---|---|
| 1 | 0.4899 | 0.0892 | 0.0379 | 0.1436 | 0.433 | 1.8 | 0.0517 | 0.71 | 0.0299 | 0.3261 |
| 2 | 0.4883 | 0.1169 | 0.0063 | 0.2268 | 0.555 | 1.7 | 0.0831 | 0.74 | -0.0515 | 0.2147 |
| 3 | 0.4893 | 0.1357 | 0.1091 | 0.2756 | 0.403 | 1.6 | 0.1240 | 0.74 | -0.0551 | 0.2894 |
| 4 | 0.4890 | 0.2588 | 0.1504 | 0.3139 | 0.216 | 1.8 | 0.1500 | 0.68 | 0.1041 | 0.5316 |
| 5 | 0.4912 | 0.2736 | 0.1640 | 0.3378 | 0.281 | 2.0 | 0.1970 | 0.66 | 0.1710 | 0.6625 |
| 6 | 0.4850 | 0.4162 | 0.3425 | 0.3593 | 0.427 | 2.6 | 0.1610 | 0.61 | 0.2963 | 0.7139 |
| **7** | **0.4753** | **0.6682** | **0.5359** | **0.3827** | **0.847** | **4.0** | **0.1120** | **0.58** | **0.3463** | **0.7497** |

TABLE-5
ACTIVITY DISTRIBUTION OF SELECTED IMIDAZOLIDINE DERIVATIVES IN TRAINING AND TEST SETS FOR EXPERIMENTAL AND QSAR-PREDICTED ANTIBACTERIAL ACTIVITIES AGAINST 14α-STEROL DEMETHYLASE PROTEIN (PDB: 1E9X)

| Compound No. | QSAR set | Activity | Predicted activity | Compound No. | QSAR set | Activity | Predicted activity |
|---|---|---|---|---|---|---|---|
| 47 | Test | 7.678 | 6.31606 | 91 | Training | 5.842 | 5.73963 |
| 52 | Training | 7.456 | 6.08613 | 7 | Training | 5.796 | 5.51206 |
| 15 | Training | 6.854 | 6.43249 | 34 | Training | 5.770 | 5.63190 |
| 21 | Training | 6.678 | 6.43466 | 37 | Training | 5.745 | 5.63453 |
| 18 | Training | 6.569 | 5.92193 | 65 | Training | 5.745 | 5.92210 |
| 58 | Training | 6.495 | 6.25710 | 100 | Test | 5.721 | 5.37510 |
| **23** | **Test** | **6.310** | **6.36390** | 77 | Training | 5.714 | 5.96302 |
| 41 | Training | 6.260 | 6.31703 | 99 | Training | 5.678 | 5.71547 |
| 85 | Training | 6.222 | 5.65748 | 92 | Training | 5.678 | 5.91066 |
| 53 | Training | 6.208 | 5.96241 | 93 | Training | 5.678 | 5.91052 |
| 56 | Training | 6.161 | 5.93204 | 102 | Training | 5.599 | 5.72868 |
| 101 | Training | 6.143 | 5.84745 | 1 | Test | 5.554 | 5.65259 |
| 8 | Training | 6.143 | 5.80201 | 29 | Training | 5.553 | 5.18437 |
| 10 | Training | 6.119 | 5.78156 | 31 | Training | 5.398 | 5.45439 |
| 73 | Training | 6.097 | 6.04494 | 48 | Training | 5.387 | 5.78258 |
| 75 | Training | 6.076 | 5.88952 | 71 | Training | 5.385 | 5.77063 |
| 95 | Test | 6.060 | 5.68322 | 19 | Training | 5.377 | 6.24444 |
| 20 | Training | 6.036 | 6.03147 | 4 | Training | 5.337 | 5.62220 |
| 22 | Training | 6.018 | 5.89941 | 11 | Test | 5.310 | 5.78656 |
| 59 | Training | 5.971 | 5.84001 | 78 | Training | 5.268 | 5.77075 |
| 79 | Training | 5.971 | 5.73220 | 14 | Training | 5.229 | 6.23511 |
| 46 | Training | 5.939 | 6.00393 | 80 | Training | 5.194 | 5.92739 |
| 68 | Training | 5.886 | 5.59611 | 72 | Training | 5.080 | 5.68869 |
| 90 | Test | 5.883 | 5.72484 | 81 | Training | 5.009 | 5.43446 |
| 83 | Training | 5.854 | 5.75245 | 13 | Training | 4.988 | 5.59434 |

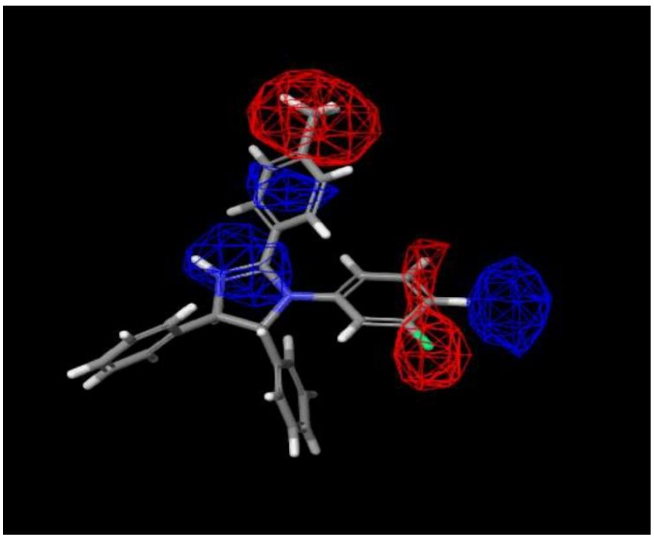


Fig. 4. 3D Gaussian electrostatic feature map showing the spatial distribution of electrostatic properties around ligand 23

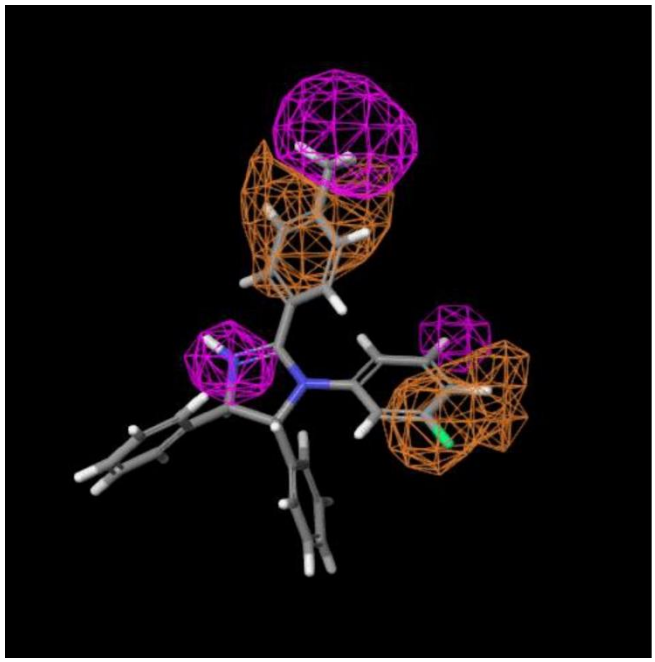


Fig. 5. 3D Gaussian hydrophobic feature map showing the spatial distribution of hydrophobic regions around ligand 23

antifungal activity. The red contours near the *meta*-fluoro substituent on the N1-linked phenyl ring and the para-methyl group of the C2-linked phenyl ring indicate regions where the electrostatic characteristics of the substituents may be less favourable. These features provide a basis for examining how changes in electronic properties influence the activity of the series.

**Hydrophobic contour map:** Fig. 5 shows the hydrophobic contour map based on ligand **23**. The orange contours near the C2 region of the imidazolidine scaffold and the *meta*-fluoro-substituted N1-linked phenyl ring suggest that hydrophobic substituents may favour antifungal activity at these positions, subject to confirmation of the contour legend. The magenta contours near the methyl substituents associated with

the C2-linked phenyl ring and the N2 position indicate regions where increased hydrophobicity may not improve activity.

### Conclusion

A series of 104 substituted imidazolidine derivatives was evaluated using computational approaches to assess their antimicrobial potential. Based on the docking results, selected compounds were synthesized and characterized. Among the evaluated derivatives, compounds **47** and **52** exhibited comparatively stronger antibacterial and antifungal activity. The molecular docking against lanosterol 14α-demethylase (CYP51; PDB ID: 1E9X) revealed favourable predicted binding interactions for these compounds, providing a possible structural basis for their antifungal activity. Pharmacophore modelling and 3D-QSAR analysis offered preliminary insights into the steric, hydrophobic and electronic features associated with biological activity, although the QSAR model showed moderate predictive performance. Compounds **47** and **52** may serve as starting points for further structural optimization and biological evaluation as potential antimicrobial agents.

## CONFLICT OF INTEREST

The authors declare that there is no conflicts of interest regarding the publication of this article.

## DECLARATION OF AI-ASSISTED TECHNOLOGIES

During the preparation of this manuscript, the authors used an AI-assisted tool(s) to improve the language and no data, results or scientific conclusions were generated by AI. All analyses, interpretations and conclusions are the authors' own. The authors reviewed and edited the content and take full responsibility for the published work.

## REFERENCES


1. G.Ş. Andrei, B.F. Andrei and P.R. Roxana, *Mini Rev. Med. Chem.*, **21**, 1380 (2021); https://doi.org/10.2174/1389557520999201209213648
2. A. Olyaei and M. Sadeghpour, *RSC Adv.*, **14**, 30758 (2024); https://doi.org/10.1039/D4RA06010E
3. Z. Özdemir, Y.N. Zenni, A. Karakurt, S. Sari, S. Saraç, M. Akdağ, I.B. Merde, D. Kart, R. Venanzoni, G.A. Flores, P. Angelini, M. Kabier, B. Mathew and S. Carradori, *Antibiotics*, **13**, 1044 (2024); https://doi.org/10.3390/antibiotics13111044
4. A. Geronikaki, V. Kartsev, P. Eleftheriou, A. Petrou, J. Glamočlija, A. Ciric and M. Soković, *Curr. Top. Med. Chem.*, **20**, 2681 (2020); https://doi.org/10.2174/1568026620666200922114735
5. D. Rani, D. Kumari, A. Bhushan, V. Jamwal, B.A. Lone, G. Lakhanpal, A. Nargotra, K. Singh and P. Gupta, *J. Mol. Struct.*, **1308**, 138105 (2024); https://doi.org/10.1016/j.molstruc.2024.138105
6. C. Sheng, Z. Miao, H. Ji, J. Yao, W. Wang, X. Che, G. Dong, J. Lü, W. Guo and W. Zhang, *Antimicrob. Agents Chemother.*, **53**, 3487 (2009); https://doi.org/10.1128/AAC.01630-08
7. F. Agili, *Molecules*, **29**, 1491 (2024); https://doi.org/10.3390/molecules29071491
8. N. Almulhim, H.M. Abd El-Lateef, M. Gouda, M.M. Khalaf and A. Abdou, *Dalton Trans.*, **54**, 8819 (2025); https://doi.org/10.1039/D5DT00551E
9. B.C. Monk, A.A. Sagatova, P. Hosseini, Y.N. Ruma, R.K. Wilson and M.V. Keniya, *Biochim. Biophys. Acta Proteins Proteom.*, **1868**, 140206 (2020); https://doi.org/10.1016/j.bbapap.2019.02.008
10. S.K. Ahmed, S. Hussein, K. Qurbani, R.H. Ibrahim, A. Fareeq, K.A. Mahmood and M.G. Mohamed, *J. Med. Surg. Public Health*, **2**, 100081 (2024); https://doi.org/10.1016/j.glmedi.2024.100081
11. E. Zarenezhad, S. Behrouz, M. Behrouz and M.N. Rad, *J. Mol. Struct.*, **1296**, 136839 (2024); https://doi.org/10.1016/j.molstruc.2023.136839
12. B. Sun, W. Huang, M. Liu and K. Lei, *J. Mol. Graph. Model.*, **77**, 1 (2017); https://doi.org/10.1016/j.jmgm.2017.07.031
13. A.K. Gopalakrishnan, S.A. Angamaly and M.P. Velayudhan, *ChemistrySelect*, **6**, 10918 (2021); https://doi.org/10.1002/slct.202102619
14. E.A. Portal, C. Farley, T. Iannetelli, J. Coelho, A. Efstratiou, S.D. Bentley, V.J. Chalker and O.B. Spiller, *Antibiotics*, **14**, 156 (2025); https://doi.org/10.3390/antibiotics14020156
15. D. Bose and R.A. Zambelli, in eds.: P. P. Srivastav, B. Srivastava and S. Karunanithi, Antimicrobial Activity of Essential Oil and Nanoemulsified Essential Oil: Minimal Inhibitory Concentration, Minimal Bacterial Concentration, Disk and Well Diffusion Methods; In: Essential Oil Extraction from Food By-Products, Springer: New York, NY, USA (2025)
16. G. Delvallez, L. Diancourt, J. Germond, P. Campagne and B. Dupuy, *Anaerobe*, **93**, 102969 (2025); https://doi.org/10.1016/j.anaerobe.2025.102969
17. H. Haridas, S. Raina, P. Das, S. Kunwar and R. Gaind, *Diagn. Microbiol. Infect. Dis.*, **114**, 117119 (2026); https://doi.org/10.1016/j.diagmicrobio.2025.117119
18. K.L. Boorn, Y.Y. Khor, E. Sweetman, F. Tan, T.A. Heard and K.A. Hammer, *J. Appl. Microbiol.*, **108**, 1534 (2010); https://doi.org/10.1111/j.1365-2672.2009.04552.x
19. R.J. Lambert and J. Pearson, *J. Appl. Microbiol.*, **88**, 784 (2000); https://doi.org/10.1046/j.1365-2672.2000.01017.x
20. C. Rodríguez-Melcón, C. Alonso-Calleja, C. García-Fernández, J. Carballo and R. Capita, *Biology*, **11**, 46 (2021); https://doi.org/10.3390/biology11010046
21. A. Singh, K. Singh, A. Sharma, K. Kaur, R. Chadha and P.M. Bedi, *Chem. Biol. Drug Des.*, **102**, 606 (2023); https://doi.org/10.1111/cbdd.14266
22. R. Becher and S.G. Wirsel, *Appl. Microbiol. Biotechnol.*, **95**, 825 (2012); https://doi.org/10.1007/s00253-012-4195-9
23. G. Madhavi Sastry, M. Adzhigirey, T. Day, R. Annabhimoju and W. Sherman, *J. Comput. Aided Mol. Des.*, **27**, 221 (2013); https://doi.org/10.1007/s10822-013-9644-8
24. M.A. Rauf, S. Zubair and A. Azhar, *Int. J. Basic Appl. Sci.*, **4**, 168 (2015); https://doi.org/10.14419/ijbas.v4i2.4123
25. D. Seeliger and B.L. de Groot, *J. Comput. Aided Mol. Des.*, **24**, 417 (2010); https://doi.org/10.1007/s10822-010-9352-6
26. S.S. Butt, Y. Badshah, M. Shabbir and M. Rafiq, *JMIR Bioinform. Biotechnol.*, **1**, e14232 (2020); https://doi.org/10.2196/14232
27. N.T. Nguyen, T.H. Nguyen, T.N. Pham, N.T. Huy, M.V. Bay, M.Q. Pham, P.C. Nam, V.V. Vu and S.T. Ngo, *J. Chem. Inf. Model.*, **60**, 204 (2020); https://doi.org/10.1021/acs.jcim.9b00778
28. T. Gaillard, *J. Chem. Inf. Model.*, **58**, 1697 (2018); https://doi.org/10.1021/acs.jcim.8b00312
29. E. Di Muzio, D. Toti and F. Polticelli, *J. Comput. Aided Mol. Des.*, **31**, 213 (2017); https://doi.org/10.1007/s10822-016-0006-1
30. S.Y. Yang, *Drug Discov. Today*, **15**, 444 (2010); https://doi.org/10.1016/j.drudis.2010.03.013
31. S.A. Khedkar, A.K. Malde, E.C. Coutinho and S. Srivastava, *Med. Chem.*, **3**, 187 (2007); https://doi.org/10.2174/157340607780059521
32. R. Tyagi, A. Singh, K.K. Chaudhary and M.K. Yadav, Pharmacophore Modeling and its Applications, In: Bioinformatics. Academic Press, pp. 269-289 (2022).
33. M.J. de Groot and S. Ekins, *Adv. Drug Deliv. Rev.*, **54**, 367 (2002); https://doi.org/10.1016/S0169-409X(02)00009-1
34. A. Kutlushina, A. Khakimova, T. Madzhidov and P. Polishchuk, *Molecules*, **23**, 3094 (2018); https://doi.org/10.3390/molecules23123094
35. C.L. Haga, C.N. Le, X.D. Yang and D.G. Phinney, *Pharmaceuticals*, 18, 440 (2025); https://doi.org/10.3390/ph18030440